IEEE Access
Multidisciplinary | Rapid Review | Open Access Journal

IEEE PHOTONICS SOCIETY SECTION

Received August 19, 2020, accepted September 22, 2020, date of publication September 30, 2020, date of current version October 12, 2020.

Digital Object Identifier 10.1109/ACCESS.2020.3027965

A Review of Using Few-Mode Fibers for Optical Sensing

ISLAM ASHRY[1], (Senior Member, IEEE), YUAN MAO[1], (Senior Member, IEEE), ABDERRAHMEN TRICHILI[1], (Member, IEEE), BIWEI WANG[1,2], TIEN KHEE NG[1], (Senior Member, IEEE), MOHAMED-SLIM ALOUINI[1], (Fellow, IEEE), AND BOON S. OOI[1], (Senior Member, IEEE)

[1] Computer, Electrical and Mathematical Sciences and Engineering Division, King Abdullah University of Science and Technology (KAUST), Thuwal 23955-6900, Saudi Arabia
[2]Department of Electronic and Information Engineering, The Hong Kong Polytechnic University, Hong Kong, SAR, China

Corresponding author: Boon S. Ooi (boon.ooi@kaust.edu.sa)

This work was supported by the King Abdullah University of Science and Technology (KAUST) under Grant BAS/1/1614-01-01, Grant GEN/1/6607-01-01, and Grant KCR/1/2081-01-01.

ABSTRACT The development of few-mode fiber (FMF) has found numerous interesting applications in optical sensing. Given the remarkable capabilities of FMF, optical sensors of novel functionalities can be deployed. Here, we review the progress on state-of-the-art technology for FMF-based optical sensing. In particular, we focus on utilizing FMF for multi-parameter and absorption-based sensing. Additionally, we summarize the trials of using FMF as a compromise between single-mode fiber (SMF) and multimode fiber (MMF) to develop optical sensors of higher signal-to-noise ratio (SNR) and spatial resolution. A final discussion on the main limitations of FMF-based sensors along with prospects for further research are presented.

INDEX TERMS Few-mode fiber, mode-division multiplexing, optical sensors, optical fiber sensors, machine learning.

I. INTRODUCTION

Fiber optic sensors (FOSs) have undergone tremendous growth and advancement over the last few decades, given their unique advantages such as immunity to electromagnetic interference, miniature sizes, large scale multiplexing, and harsh environment operation [1], [2]. Such unique capabilities make fiber optics the preferred sensing platform in a myriad of fields, including oil and gas industry [3], structural health monitoring [4], healthcare sector [5], among others [6], [7]. Generally, FOSs can be classified based on the measurand's spatial distribution to include point, integrated, quasi-distributed, and distributed sensors [8]. The majority of such FOSs are based on single-mode fiber (SMF), which can be standard SMF, photonic-crystal fiber (PCF) [9], or polarization-maintaining fiber (PMF) [10]. Other sensing applications that require utilizing high optical power deploy standard multimode fiber (MMF), which has a high power threshold of nonlinearity [2].

The associate editor coordinating the review of this manuscript and approving it for publication was Rene Essiambre.

Since SMF supports propagating a single spatial mode, the operation characteristics of SMF-based sensors cannot be easily tuned. Additionally, a sensing segment along SMF is typically incapable of discriminating multiple sensing parameters. For instance, the SMF-based Brillouin optical time-domain reflectometer (BOTDR) typically resolves either strain or temperature along the fiber [2].

On the other side of MMF-based sensing, using MMF as a solution for multi-parameter sensing is also not recommended due to the strong and often uncontrollable intermodal coupling within the MMF. This intermodal coupling is an inevitable source of noise in most of the MMF-based sensors [11], which typically requires complicated systems to be controlled [12]. Another example is the mode-dependent absorption sensing, which relies on monitoring the intensity change of a spatial mode, following the mode's interaction with a measurand. In an MMF, the modes' intensities keep rapidly changing along the fiber because of intermodal coupling, even without interaction with a measurand. Thus, the effect of intermodal coupling can significantly degrade the performance of MMF-based mode-dependent

absorption sensors. As a result, there is a strong motivation to develop compromise FOSs offering functionalities that cannot be easily achieved using SMF- and MMF-based sensors.

Few-mode fiber (FMF) is an ideal compromise between SMF and MMF, which can develop optical sensors with remarkable capabilities [13]–[16]. An FMF can support the propagation of a few guided modes, up to a few tens, and each mode can be used individually for optical sensing [17]. In contrast, a typical MMF can carry a few hundreds of modes, and all the modes combined serve for sensing. It is easier to control/limit intermodal coupling in FMF, compared with MMF. This is because the most straightforward method to reduce intermodal coupling is to increase the difference between the propagation constant values of the modes [18]. Increasing the index difference between different modes is relatively easy to achieve for FMF, which has a limited number of modes, compared to MMF.

FMFs have recently benefited optical sensing for two main reasons. On the one hand, various LP modes within an FMF respond differently when subjected to external parameters such as temperature, pressure, gas, etc. Consequently, monitoring the various responses of the modes enables simultaneous measurements of multiple parameters and develops new sensing techniques [16], [19]. On the other hand, FMFs can offer traditional optical fiber sensors with higher signal-to-noise ratio (SNR) levels than those designed using the standard SMFs and MMFs. This is because FMFs mitigate intermodal coupling and modal dispersion that occur in the typical MMFs, and FMFs further have higher power thresholds of nonlinearity, compared with the standard SMFs [20], [21].

In this article, we review the different approaches and types of FMF-based optical sensors. We first define and discuss the mode transfer and calibration matrices, essentially used when designing FMF-based senors. Next, we follow Fig. 1 to summarize the various FMF-based sensing techniques. Considering the various reactions of spatial modes to external parameters, we summarize the different trials of multi-parameter sensing using FMFs. Afterward, within the same sensing category, we discuss the possibility of using the mode-dependent absorption in FMFs to deploy extremely large-scale sensing networks and to reconstruct spatial distributions of gases that diffuse into an FMF, functionalities which are almost impractical to realize using standard SMF/MMF. We then review the experiments that enhance the performances of fiber optic sensors using FMF, as a compromise between utilizing SMF and MMF in such sensors. Finally, we point out the main limitations of FMF-based sensors and future directions of related research. This review aims to provide a framework for utilizing FMFs in advancing FOSs.

II. MODE TRANSFER MATRIX AND CALIBRATION MATRIX FOR FMF-BASED SENSING

FMF imperfections, including index inhomogeneity, bends, and core ellipticity, cause coupling between modes, a phenomenon known as intermodal coupling [22]. The intermodal

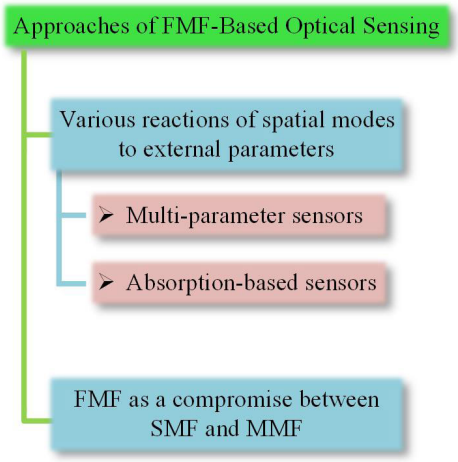

FIGURE 1. The various approaches and types of FMF-based sensing.

coupling is described using a mode transfer matrix, which maps any field launched into one end of the FMF with the corresponding field generated at the other end [23], [24]. The transfer matrix comprises the coupling amplitudes and phases (complex coupling coefficients) of the all modes supported by the FMF. Although it is important to investigate the mode transfer matrix when designing an FMF-based sensor, the mode transfer matrix has only been included in a limited way.

The mode transfer matrix can be measured experimentally using an optical vector network analyzer with spatial-diversity [25], spatial light modulator (SLM) [26], or multiple-input multiple-output (MIMO) processing [27]. Alternatively, the following approach is typically adopted to model the FMF's transfer matrix [23], [24]. In this model, the FMF is assumed to be a weakly guiding fiber, which supports propagating a set of linearly polarized (LP) modes. To simplify our analysis, we initially focus on the coupling between the spatial modes without considering the coupling between the polarization modes. The coupled mode equation between the LP_{lm} and $LP_{l'm'}$ modes along the direction of light propagation (z) can be expressed as [23], [28]:

$$\frac{da_{lm}}{dz} = -j\beta_{lm}a_{lm} + \sum_{l'm' \neq lm} C_{lm,l'm'}a_{l'm'}, \tag{1}$$

where a_{lm} and β_{lm} are the complex mode amplitude and the propagation constant of the LP_{lm} mode, respectively. The coupling coefficient $C_{lm,l'm'}$ between the LP_{lm} and $LP_{l'm'}$ modes is defined as [23], [24]:

$$C_{lm,l'm'} = \frac{k_0 c\varepsilon_0}{4j} \iint \Delta n^2(x,y) E^*_{lm}(x,y) E_{l'm'}(x,y) dxdy, \tag{2}$$

where k_0 denotes the free space wavenumber, c is the speed of light in vacuum, ϵ_0 is the free space permittivity, and $E_{lm}(x,y)$ is the field distribution of the LP_{lm} mode. The refractive index perturbation $\Delta n^2(x,y)$, which results in intermodal coupling, may be caused by the residual birefringence, bending, core

ellipticity, etc. Calculating $\Delta n^2(x, y)$, caused by different perturbation sources, is described in [11].

In this model, the FMF is divided into M sections, where the index perturbation is assumed to be independent of z within each section [23]. Using this assumption, Eq. 1 can be solved to give the following solution in a matrix form for the i^{th} section:

$$\hat{A}(L_{seg}) = \exp((-j\hat{\Gamma} + \hat{C}_i)L_{seg})\hat{A}(0), \tag{3}$$

where $\hat{A}$ is a complex column vector containing the complex amplitudes of the propagating modes, L_{seg} denotes the section length, and $\hat{\Gamma}$ is a diagonal matrix containing the propagation constants of the all modes supported by the FMF. $\hat{C}_i$ is a hollow square coupling matrix describing coupling between guided modes, where its coefficients are calculated using Eq. 2. Based on Eqs. 1 to 3, the complete transfer matrix is therefore given as a product of M segment matrices:

$$\hat{T} = \prod_{i=1}^{M}[\exp((-j\hat{\Gamma} + \hat{C}_i)L_{seg})], \tag{4}$$

where $L_{seg} = L / M$, and L is the length of the FMF. The transfer matrix is square of a rank equals the number of guided modes in the FMF. In case of further accounting the coupling between the polarization modes (i.e., modes of two orthogonal polarization states), the transfer matrix of Eq. 4 has to be extended, as described in [23].

For the mode-dependent interferometric and absorption-based optical sensors, the transfer matrix should be considered and inverted to compensate for the modes' power and phase fluctuations. The inversion can be achieved using MIMO processing [27], a SLM [26], or modeling [14]. The impact of intermodal coupling might be easily compensated or even neglected for the weak coupling regime [14], [22], where the number of guided modes is small, the differences between the modes' propagation constants are large, and the fiber imperfections are minimized. Consequently, step-index two-mode fiber is commonly used for optical sensing. On the contrary, when the intermodal coupling is strong and rapid between many modes, it is difficult to compensate for the intermodal coupling. Under the latter scenario, the intermodal coupling would enlarge the measurement uncertainty producing unreliable sensing.

When using the mode-based multi-parameter sensing, the spectral characteristics of the individual modes are typically monitored. In this case, the power/phase fluctuations of the modes do not have substantial impacts on the sensor performance, especially for weakly-coupled FMF sensors of a low mode-dependent loss. Instead, the conditions of the sensor calibration matrix $\hat{\kappa}$ is more important [29]. The calibration matrix of an FMF-based sensor comprises the sensitivity values, such as temperature and strain sensitivity, of the FMF's modes. Assuming there are M measurands, the FMF should at least support the propagation of M modes, without considering mode-degeneracy, in order to discriminate the measurands. Under this scenario, the calibration matrix $\hat{\kappa}$ can

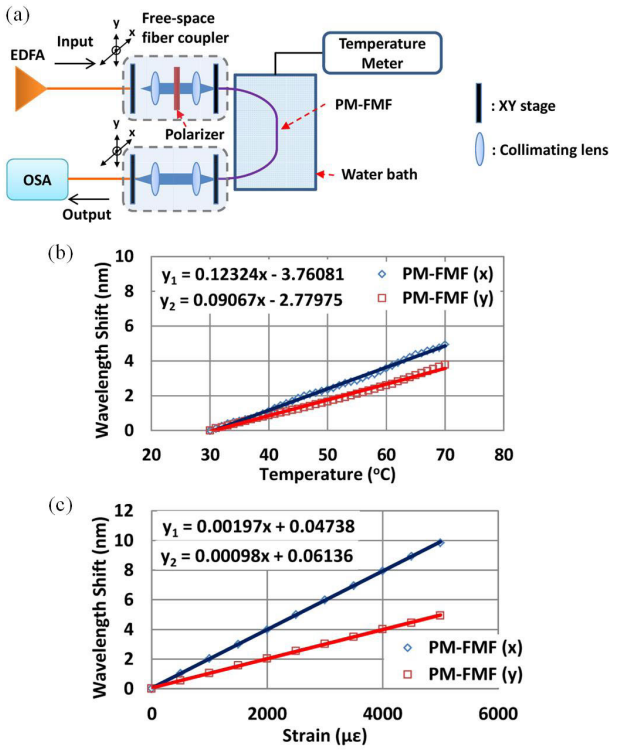

FIGURE 2. (a) Schematic of the PM-FMF interferometer temperature sensor. Wavelength shift of the transmission minimum against temperature (b) and strain (c) [13].

be defined as:

$$\hat{\kappa} = \begin{pmatrix} \kappa_{Meas.\ 1}^{Mode\ 1} & \cdots & \kappa_{Meas.\ M}^{Mode\ 1} \\ \vdots & \ddots & \vdots \\ \kappa_{Meas.\ 1}^{Mode\ M} & \cdots & \kappa_{Meas.\ M}^{Mode\ M} \end{pmatrix}, \tag{5}$$

where $\kappa_{Meas.\ m}^{Mode\ n}$ is the sensitivity of the n^{th} mode to the m^{th} measurand, and $n,\ m = 1, 2, \cdots M$. The calibration matrix $\hat{\kappa}$ should be safely away from being singular; otherwise, $\hat{\kappa}$ would enlarge the measurement inaccuracy, and the FMF-based sensor would be useless. In mathematics, the condition number of the calibration matrix is typically used to estimate the sensitivity of the solution of a system of linear equations [29]. The smaller the condition number of the calibration matrix, the higher the discrimination accuracy. Additionally, the calibration matrix has to be modified if the FMF-based sensor has a cross-sensitivity [30]. In other words, a sensitivity value is a function of more than one measurand. Consequently, investigating the calibration matrix is crucially important when designing a mode-based multi-parameter sensor.

III. VARIOUS REACTIONS OF SPATIAL MODES TO EXTERNAL PARAMETERS

A. MULTI-PARAMETER SENSING USING FMF

When an FMF supports propagating N modes, without considering mode-degeneracy, the FMF can sense in principle N different parameters. The operation principle of FMF-based

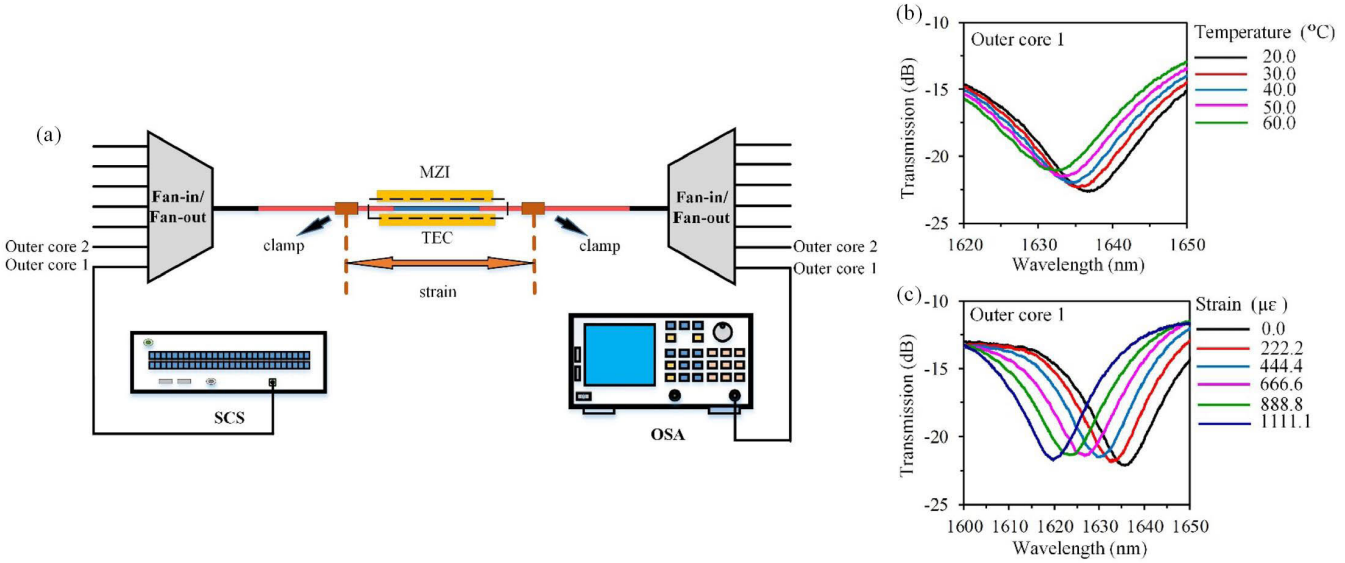

FIGURE 3. **(a) Experimental setup of measuring temperature and strain using FM-MCF based MZIs. The Wavelength shift of outer core 1 as temperature (b) or strain (c) varies [16].**

multi-parameter sensors is mainly attributed to the different effective refractive index (n_{eff}) values of the non-degenerate spatial modes [31]. Consequently, for instance, the Bragg wavelength of a fiber Bragg grating (FBG) or Brillouin frequency shift (BFS) becomes highly mode-dependent in an FMF. In other words, each spatial mode has a particular distinctive sensitivity for measurands. Using the calibration matrix [32], multi-parameter discrimination can be realized. In this subsection, we summarize the trials of developing discrete FMF-based multi-parameter sensors, and then we discuss the distributed counterparts. Li *et al.* designed an interferometric sensor using a polarization-maintaining FMF (PM-FMF) such that the signals interference occurs between the spatial modes [13]. The used experimental setup is shown schematically in Fig. 2(a) where an erbium-doped fiber amplifier (EDFA) generates a broadband spectrum light coupled to a SMF. This light is transferred from the SMF to the PM-FMF through the offset launch technique. The PM-FMF supports propagating the LP_{01} and LP_{11} mode, and by controlling the offset between the axes of the SMF and PM-FMF, the two modes are equally excited within the latter fiber. The PM-FMF is immersed in a water bath of controllable temperature, and also a strain, not shown in Fig. 2(a), can be applied to the fiber. The output light from the distal end of the PM-FMF is coupled again to a SMF, and the transmitted light is analyzed with an optical spectrum analyzer (OSA). While changing the water bath temperature, the authors investigated the transmission spectra of the PM-FMF intermodal interferometer when injecting different light polarization states. For the LP_{01x}-LP_{11x} and LP_{01y}-LP_{11y} interference, the measured temperature coefficients are 0.123 nm/°C and 0.091 nm/°C, respectively [Fig. 2(b)]. On the other hand, when stretching the PM-FMF, the strain coefficients equal 1.97 pm/$\mu\varepsilon$ and 0.98 pm/$\mu\varepsilon$ for the LP_{01x}-LP_{11x} and LP_{01y}-LP_{11y} intermodal interference, respectively [Fig. 2(c)]. The intermodal interferometer has much less temperature sensitivity, whose temperature coefficients are 7% (LP_{01x}-LP_{11x}) and 5% (LP_{01y}-LP_{11y}) of that of the corresponding (LP_{01x}-LP_{01y}) polarimetric interferometer. This is likely attributed to the large modal birefringence in the PM-FMF, compared with the polarimetric birefringence. In contrast, the intermodal interferometer shows a relatively high strain sensitivity, which is comparable to that of a special-designed PM-PCF-based strain sensor [33]. Consequently, the PM-FMF-based intermodal interferometer is considered an efficient temperature-insensitive strain sensor. Combining the intermodal interference with the typical polarimetric interference, which are normally very different, can result in multi-parameter discrimination. Although the authors did not provide experimental results for simultaneous temperature-strain sensing, the approach would be straightforward. In particular, the temperature-insensitive intermodal interferometer can be used as a reference strain sensor when using the polarimetric interferometer for temperature and strain measurements.

Another trial was reported in [16] for temperature and strain discriminative sensing, using paralleled Mach-Zehnder interferometers (MZIs) in a few-mode multicore fiber (FM-MCF). The used experimental setup is shown in Fig. 3(a) where a supercontinuum optical laser (SCS, from YSL Photonics) injects light into a spatial fan-in/fan-out device such that its output port is a single-mode MCF. The FM-MCF is firstly rotated by 3° and then "sandwiched" between two single-mode MCFs, via fusion splicing. This structure excites many modes in the outer cores of the FM-MCF. Since the effective refractive indices of the guided

spatial modes are different, the modes' optical path differences accumulate over the FM-MCF to create a MZI in the outer cores of the FM-MCF. The optical spectra of the light transmitted through the FM-MCF is analyzed using an OSA.

Fig. 3(b) shows the measured wavelength shift of the transmitted light through the outer core 1 as temperature changes, when the strain equals 0.0 $\mu\varepsilon$. Similarly, when fixing the temperature at 30 °C, Fig. 3(c) shows the relationship between the wavelength shift and strain for the light transmitted through the same outer core (core 1). It was found that the temperature sensitivities equal 105.8 pm/°C and 223.6 pm/°C while the strain sensitivities are 13.96 pm/$\mu\varepsilon$ and 11.7 pm/$\mu\varepsilon$ for the outer core 1 and core 2, respectively. Since these two outer cores have different responses to temperature and strain, they can be discriminated by using the calibration matrix of the cores, rather than the modes. The condition number of the calibration matrix was calculated to be 32, which is smaller than those of the counterpart sensors designed using SMF/MMF [34], [35]. Consequently, this design offers acceptable relative errors of 4.8% and 8.7% for temperature and strain, respectively.

Another approach for multi-parameter sensing using FMF is reported in [36]. In this work, simultaneous directional curvature and temperature are monitored using a tilted FBG written in an FMF that supports propagating four modes (LP_{01}, LP_{11}, LP_{02}, and LP_{21}). The LP_{11} mode's resonance intensity depth in the tilted FM-FBG exhibits a curvature sensitivity, while temperature tunes the Bragg wavelength of the LP_{11} mode. Such observation facilitates the hybrid sensing of the curvature and temperature.

The tilted FM-FBG is shown schematically in Fig. 4(a). The LP_{11} mode's transmission spectra of a 1° tilted FM-FBG decreases against the applied curvature, with a slight change in the resonance wavelength [Fig. 4(b)]. In contrast, Fig. 4(c) shows a clear change of the LP_{11} mode's Bragg wavelength against temperature, with minimal variations in resonance depth. This reported sensor offers discriminated measurements of curvature and temperature with 9.15×10^{-4} m^{-1} and 0.952 °C resolution, respectively. A 2×2 calibration matrix describes this sensor, which includes the sensitivity coefficients that link the curvature and temperature changes with the variations of resonance depth and Bragg wavelength. However, this work lacks quantifying the relative error of the curvature and temperature measurements. Calculating the measurement uncertainty and the condition number of the calibration matrix provide credibility in the performance of the multi-parameter sensor. Another new approach for distinguishing temperature and strain using a FBG written in a panda-type PM-FMF was demonstrated in [15]. It was observed that the intensity of the reflected light from the FBG in this design varies sinusoidally with temperature and strain. This intensity variation provides a phase that changes linearly with temperature and strain. Thus, full discrimination of the two sensing parameters can be achieved via wavelength and phase modulation. The FMF in this experiment supports propagating the LP_{01} and LP_{11}

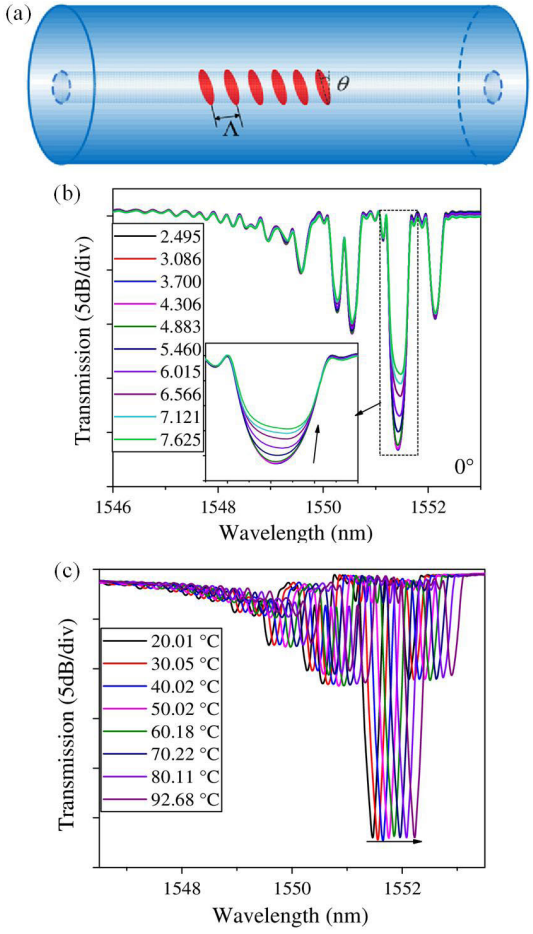

FIGURE 4. (a) Schematic of the tilted FM-FBG. Transmission spectra of the 1° tilted FM-FBG at different curvature (b) and temperature (c) values [36].

mode, and the polarization state of the launched light is controlled using a polarization controller (PC). As shown in the representative examples of Fig. 5(a)/5(b), the reflection spectra (denoted as i, ii, iii, and iv) of the LP_{01} and LP_{11} mode and their combinations at different polarization states change with temperature/strain. Focusing on the intensity of peak (iii), it exhibits large fluctuations with temperature and strain. This simultaneous wavelength shift and interrogated phase change of peak (iii) can offer dual-sensing of temperature and strain, as shown in Fig. 5(c). To evaluate the performance of this sensing approach, the efficiency of discriminating the temperature and strain were investigated. This sensor offers a 98% discrimination efficiency, which is better than most counterpart methods reported in the literature [37], [38]. Yang *et al.* experimentally demonstrated simultaneous sensing of refractive index (RI) and temperature of a solution using a cladless FBG written in a two-mode fiber [30]. The Bragg wavelengths of the two LP modes (LP_{01} and LP_{11}) have different sensitivities to the changes of RI and temperature. Fig. 6(a) shows the shifts of the Bragg wavelengths associated with the LP_{01} and LP_{11} modes, as the RI changes.

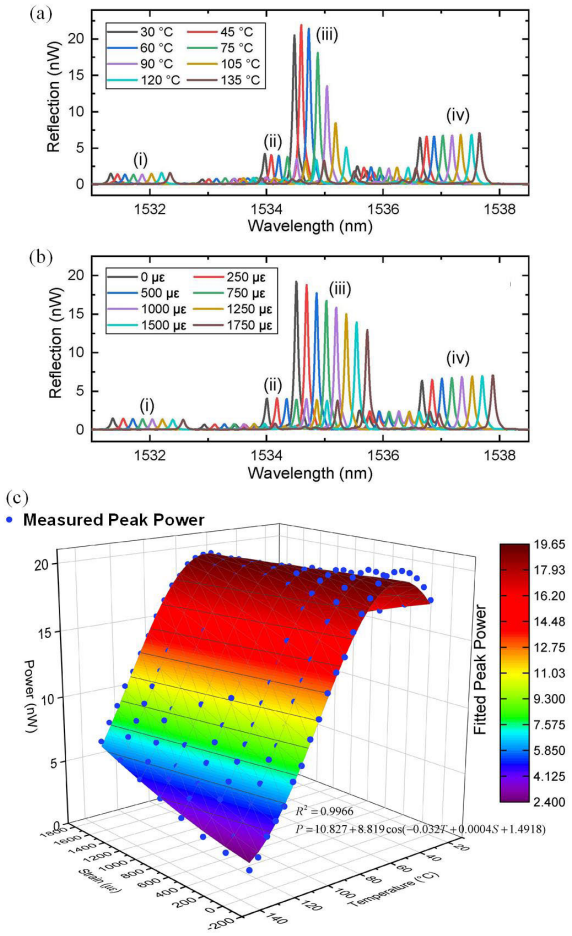

FIGURE 5. **Reflection spectra of the FBG written in PM-FMF with changing temperature (a) and strain (b). (c) Intensity response of peak (iii) with simultaneous temperature and strain change [15].**

Obviously, the two modes exhibit different sensitivities. Similarly, the FBG reflection spectra of the LP_{01} and LP_{11} modes behave differently with changing the solution's temperature [Fig. 6(b)]. However, the authors find that the temperature sensitivities of the LP_{01} and LP_{11} modes are functions of the RI, which requires modifying the calibration matrix [Eq. 5], as follows:

$$\begin{pmatrix} \Delta\lambda^{01} \\ \Delta\lambda^{11} \\ \Delta\lambda \end{pmatrix} = \begin{pmatrix} \kappa_\alpha^{01} & \kappa_T^{01} & \kappa_n^{01} \\ \kappa_\alpha^{11} & \kappa_T^{11} & \kappa_n^{11} \\ 0 & 0 & \kappa_n^{01} - \kappa_n^{11} \end{pmatrix} \cdot \begin{pmatrix} \Delta\alpha \\ \Delta T \\ \Delta n \end{pmatrix}, \quad (6)$$

where $\Delta\lambda^{01}$ and $\Delta\lambda^{11}$ respectively denote the Bragg wavelength shifts of the individual LP_{01} and LP_{11} modes, and $\Delta\lambda$ is the spacing between the Bragg wavelengths of the LP_{01} and LP_{11} modes. κ_α^{lm}, κ_T^{lm}, and κ_n^{lm} represent the cross-sensitivity between the temperature and RI, temperature sensitivity, and RI sensitivity of the LP_{lm} mode, $lm = 01, 11$, respectively. The change in temperature and ambient RI are correspondingly denoted as ΔT and Δn, and $\Delta\alpha = \Delta T \Delta n$. By inverting the 3×3 modified calibration matrix, the RI and temperature can be simultaneously measured with $\pm 8 \times 10^{-4}$ RIU and ± 1 °C deviations, respectively, Regarding optical fiber distributed sensors, Brillouin scattering based sensors have a long-standing challenge of discriminating temperature and strain along SMF [2]. This challenge exists because the BFS is dependent on temperature and strain along the fiber length. Therefore, in order to simultaneously measure temperature and strain, an additional Raman-based distributed temperature sensor is typically installed to offer temperature as a reference for the SMF-based Brillouin sensor. Since the Raman signal is very weak (60–70 dB weaker than the input pump power) [39], high power is required to be launched into the optical fiber in order to have a reasonable SNR. Consequently, to avoid exceeding the fiber's threshold power of nonlinearity, MMF is the preferred platform for the Raman-based temperature sensors [40]. Installing SMF and MMF to offer a hybrid temperature-strain sensor increases the system complexity and cost.

A cyclic Simplex coding was used to design a Raman-based DTS along a SMF [41]. This technique could be combined with the SMF-based BOTDR to discriminate temperature and strain along the SMF without the need for installing additional MMF for temperature sensing. However, including the cyclic Simplex coding with the BOTDR would sophisticate the multi-parameter sensing system. Another trial was reported in [42] for using a Brillouin optical time-domain analysis (BOTDA) system, which employs two different wavelengths to simultaneously resolve temperature and strain along a bending-loss insensitive SMF. The two wavelengths should be widely spectrally separated, e.g., 850 nm and 1550 nm. It was found that the ratio between the strain sensitivity is different from that between the temperature sensitivity at the two wavelengths. This leads to discriminating temperature and strain along the fiber. However, the speciality SMF used in the experimental setup makes the system unpopular and utilizing two wavelengths relatively complicates the sensing system.

FMF solves this dilemma of discriminating temperature and strain in Brillouin-based distributed sensors. This can be realized because spatial modes in FMF have different sensitivity values to temperature and strain, as demonstrated in the following matrix representation [32]:

$$\begin{pmatrix} \Delta\upsilon_B^1 \\ \vdots \\ \Delta\upsilon_B^n \\ \vdots \\ \Delta\upsilon_B^N \end{pmatrix} = \begin{pmatrix} \kappa_{\upsilon T}^1 & \kappa_{\upsilon\varepsilon}^1 \\ \vdots & \vdots \\ \kappa_{\upsilon T}^n & \kappa_{\upsilon\varepsilon}^n \\ \vdots & \vdots \\ \kappa_{\upsilon T}^N & \kappa_{\upsilon\varepsilon}^N \end{pmatrix} \cdot \begin{pmatrix} \Delta T \\ \Delta\varepsilon \end{pmatrix}, \quad (7)$$

where $\Delta\upsilon_B^n$ $(n = 1, 2, \cdots N)$ is the BFS of the n-th mode, $\kappa_{\upsilon T}^n$, $\kappa_{\upsilon\varepsilon}^n$ $(n = 1, 2, \cdots N)$ are respectively the temperature and strain sensitivity of the n-th mode, and $\Delta T/\Delta\varepsilon$ are the change of temperature/strain. Using Eq. 7, a two-mode fiber should be sufficient to simultaneously sense the temperature and strain along the fiber.

Weng *et al.* introduced a single-end FMF-based distributed BOTDR that can discriminate temperature and strain

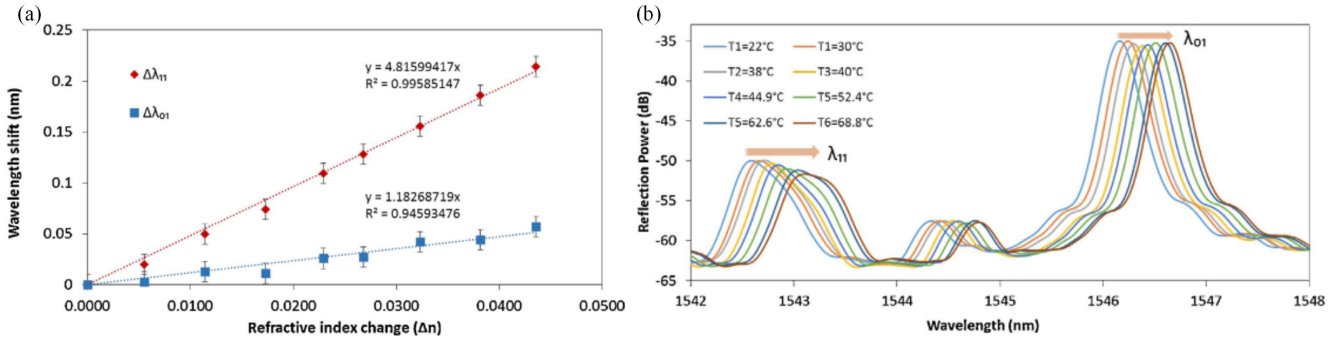

FIGURE 6. (a) Changes of the Bragg wavelengths associated with the LP_{01} and LP_{11} modes with the variations of the solution's RI. (b) FBG reflection spectra of the two modes as the solution's temperature changes [30].

measurements along an FMF [32]. Using a heterodyne detection technique, the presented BOTDR exhibits similar performance as the two-end methods, such as the BOTDA, but with a simpler setup and lower cost. In this system, a 1550 nm distributed feedback (DFB) laser diode (LD) launches the individual spatial modes, using a mode MUX, into a two-mode optical fiber. The backscattered Brillouin signals of the spatial modes are decomposed with a mode DEMUX to be detected via a heterodyne receiver. Figures 7(a) and 7(b) show the BFS-dependence of the LP_{01} and LP_{11} modes on temperature and strain, respectively. Obviously, the LP_{01} and LP_{11} modes have various sensing coefficients to the temperature and strain. Using Eq. 7, the two measurands can be simultaneously monitored. It is worth highlighting that the maximum errors for the temperature and strain measurements were estimated when only considering the uncertainty induced by the BFSs from different modes and ignoring the uncertainty of the temperature and strain sensitivity values. Following this assumption, ± 1.7 °C and ± 39 $\mu\varepsilon$ temperature and strain accuracy are estimated, respectively. A similar technique of using a 5-mode FMF and the BOTDA method to discriminate temperature and strain was successfully presented in [13]. In this work, the spatial modes were launched into the FMF as a pulsed-wave-pump and a continuous-wave (CW) probe. Again, the LP_{01} and LP_{11} modes experimentally exhibit different temperature and strain sensitivities, which allow the hybrid-sensing procedure. This article offers a proof-of-concept demonstration for temperature and strain discrimination using the FMF-based BOTDA; however, further study is needed to quantify the measurement uncertainty of the reported sensor. In other words, the impact of the calibration matrix's condition on the temperature/strain measurements is ignored in this study.

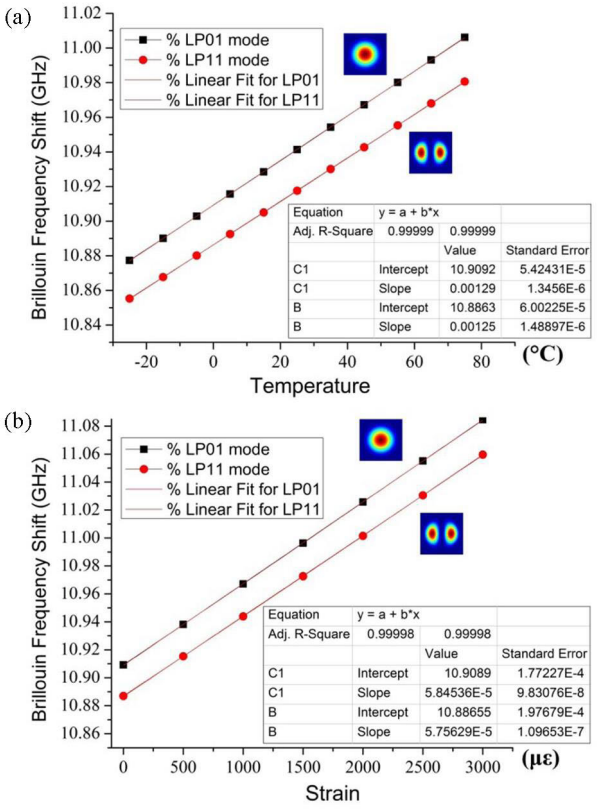

FIGURE 7. Calibration of temperature (a) and strain (b) sensing coefficients for the LP_{01} and LP_{11} modes [32]. Adj., Adjusted.

B. ABSORPTION-BASED SENSING USING FMF

The typical operation principle of fiber optic absorption-based sensors relies on monitoring optical attenuation resulted from the interaction of light, propagating within an optical fiber, with absorptive material. The fiber optic sensing segment is designed to reinforce such interaction based on the absorptive material's nature. In case that the absorptive material cannot diffuse into the optical fiber, for instance, fiber taper or D-shaped fiber are conventionally used to offer interaction between the evanescent field in the fiber's cladding region and absorptive material [43], [44].

Focusing on absorption-based sensors designed using FMFs, different LP modes propagating within an FMF possess various spatial distributions. Consequently, spatial overlaps between light propagating within the FMF-based sensing segment and absorptive material should become highly mode-dependent. By scanning interrogation signals in the mode-domain via injecting different LP modes or their superposition into an FMF, novel sensing functionalities can be designed. Figure 8 shows a representative example of an FMF

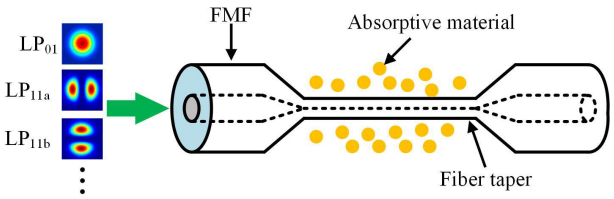

FIGURE 8. An illustration of the use of an FMF taper as a sensing segment.

taper that acts as a sensing segment in an absorption-based optical sensor. For simplicity, assuming that all spatial modes have the same polarization within the FMF. The optical field in the fiber $E(x, y)$ can be represented as a superposition of the LP modes:

$$\begin{cases} E(x,y) = \sum_{lm} a^{lm} E_{lm(x,y)}. \\ l = 0, 1, \ldots \\ m = 1, 2, \ldots \end{cases} \tag{8}$$

By changing the values of the complex coefficients a^{lm}, an infinite number of the combinations of LP modes can be injected into the FMF-based sensing segment, in principle. Such a unique option can reconstruct the spatial distribution of absorptive material within and around the FMF. Ashry *et al.* demonstrated the possibility of reconstructing the spatial distributions of absorptive chemicals that diffuse into an FMF [19]. This is accomplished by measuring the optical attenuation of multiple LP modes in the fiber and utilizing a constrained nonlinear optimization algorithm. As a representative practical implementation, the authors of this work considered the example of hydrogen diffusion into a silica FMF that supports propagating 17 LP modes [Fig. 9(a)]. Figure 9(b) shows the significant differences in the radial optical intensity distributions of the LP_{01}, LP_{02}, and LP_{03} mode within the FMF. Such variations in the modes' spatial intensity distributions originate the mode-dependent loss when interacting with the hydrogen that diffuses into the FMF. The reported algorithm efficiently reconstructs arbitrary hydrogen distribution profiles, as the shown examples in Figs. 9(c) and 9(d). Regardless of the initial guess of the gas spatial distribution (dashed black lines), the reconstructed spatial profiles (red squares) resemble the original ones (solid blue lines) with reasonable accuracy, as presented in Figs. 9(c) and 9(d). It is worth mentioning that the original gas spatial distributions were theoretically and arbitrary selected, i.e., no experimental reference sensor was used to measure the original distributions. Additionally, the authors investigated the impact of intermodal coupling on the reconstruction process. Even in a strong intermodal coupling regime, quite reasonable results were achieved.

There are many applications for reconstructing spatial distributions of gases diffusing into fibers [45]. For example, in an oil-gas well, fiber optic sensors operate in extremely challenging environments of temperature and pressure as high as 300 °C and 2000 bar, respectively [3].

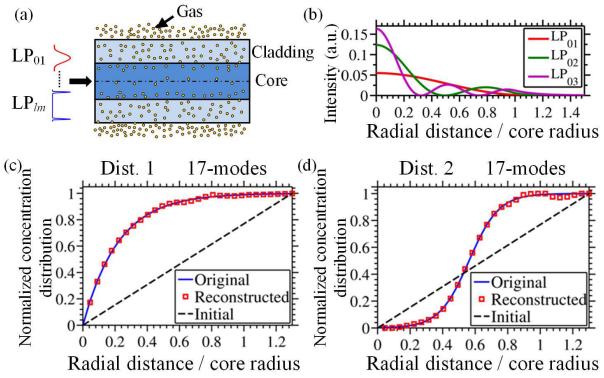

FIGURE 9. (a) Hydrogen diffusion into an FMF. (b) Radial intensity distribution of the LP_{01}, LP_{02}, and LP_{03} mode. Reconstruction of hydrogen spatial distribution into the FMF for (c) Dist. 1 and (d) Dist.2 arbitrary spatial original profiles [19]. Dist., Distribution.

Such harsh environments may result in hydrogen darkening, which is a gradual temporal diffusion of hydrogen into the optical fiber. The hydrogen darkening changes the fiber's refractive index and significantly attenuates sensing interrogation signals. Reconstructing spatial distributions of hydrogen diffusing into fibers is important in studying fiber losses [46], photosensitivity [47], and drift in the wavelength of FBGs [48]. Another trial was reported in [14] for using an FMF and mode-division-multiplexing (MDM) to construct an absorption-based quasi-distributed sensing network that combines high sensitivity with large-scale multiplexing. This remarkable design is achieved by utilizing the low-loss fundamental mode (LP_{01}) to transmit the interrogation signal along the FMF and the high-attenuation LP_{02} mode for sensing. The operation principle of this sensing network is summarized in Fig. 10(a) where the fiber Bragg grating (FBG1) is used with adaptive optics to ensure the interrogation signal is purely the LP_{01} mode. Afterwards, the FBG2 converts part of the incident LP_{01} signal into the LP_{02} mode for sensing. The two sensing FBGs (FBG3 and FBG4) reflect only the LP_{02} mode, and the ratio between their reflected signals is linked to the attenuation within the sensing segment. The remaining power of the incident LP_{01} mode continues to serve as the interrogation signal in the remaining network. As Fig. 10(b) shows, when ignoring intermodal coupling within the network, the maximum number of sensors N_{max} that can be included in this network is 561 when the reflection coefficients of FBG3 and FBG4 respectively equal 5.95% and 20.80%. Afterwards, the mode transfer matrix was thoroughly considered when modeling the FMF-based sensing network. The network can comprise up to 41 sensors in the strong coupling regime, where the variance S represents the strength of intermodal coupling [Fig. 10(c)].

IV. FMF AS A COMPROMISE BETWEEN STANDARD SMF AND MMF

Increasing the input power in a SMF is mainly limited by nonlinear fiber effects, including self-phase modulation, cross-phase modulation, four-wave mixing, stimulated

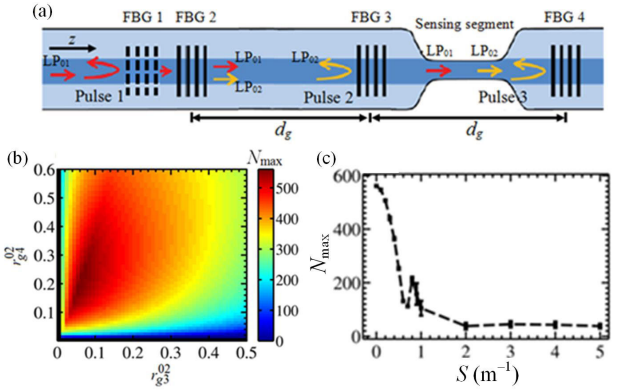

FIGURE 10. (a) Schematic of the FMF-based absorption sensor. Maximum number of sensors allowed for the ideal quasi-distributed sensing network (b) and at different intermodal coupling strength values (c) [14].

Brillouin scattering, and stimulated Raman scattering (SRS) [49]. In optical time-domain reflectometry (OTDR) based distributed FOSs, for instance, optical pulses of meter-scale resolution are typically launched into the fiber. The pump power of these optical pulses is mainly limited by the SRS threshold, P_{th}, which can be expressed as [20], [49]:

$$P_{th} = 20\frac{A_{eff}}{g_R L_{eff}}, \tag{9}$$

where A_{eff} is the mode effective area, g_R denotes the Raman gain coefficient, and L_{eff} represents the effective fiber length.

Compared to the standard SMF, FMF generally supports higher input powers because FMF has a relatively larger mode effective area, which allows a higher nonlinearity power threshold [Eq. 9]. On the other hand, FMF is less sensitive to intermodal coupling, and it mitigates modal dispersion, compared with the standard MMF. Enhancing the input power levels and reducing the effect of modal dispersion through the use of FMF enable developing FOSs with improved characteristics. For example, compared with SMF- and MMF-based distributed FOSs, FMF can extend the sensing range of distributed FOSs while maintaining reasonable spatial resolution values [50]. The authors of [20] investigated the performance of Raman-based distributed temperature sensor (DTS) using a 2-mode FMF and a 4-mode FMF, both operating in the quasi-single mode (QSM) state such that only the LP_{01} mode is excited at the fiber input. Figure 11(a) shows a representative example of the temperature-distance trace when using the 2-mode FMF. The authors of this work reported a temperature resolution of about 7 °C and 6 °C for the 2-mode and the 4-mode FMF, respectively, compared to a resolution of about 10 °C for a standard SMF, at the same distance (20 km) and for the same spatial resolution (3 m) [Fig. 11(b)]. The 2-mode FMF outperforms the 4-mode FMF since the 2-mode one has smaller losses when it is spliced with a SMF for the QSM operation purpose. Meanwhile, the 2-mode FMF can offer reliable temperature measurements with a high spatial resolution (3 m) at a sensing range of 20 km, which is difficult to be achieved via the standard MMF because of modal dispersion.

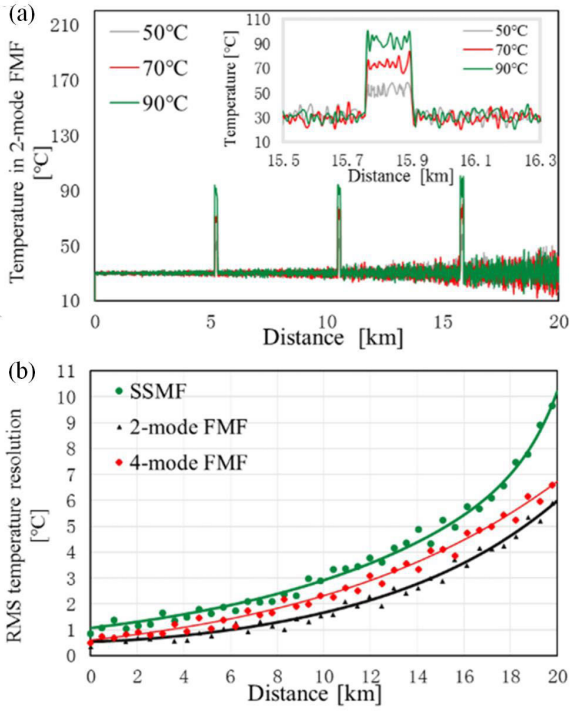

FIGURE 11. (a) Temperature-distance profile recorded when using the 2-mode FMF. (b) RMS temperature resolutions of different fiber types [20].

One major disadvantage of this work is that the temperature resolution of the 2-mode FMF-based Raman sensor is ∼6 °C, at 20 km distance, which is relatively low compared with that of the MMF-based DTS [2]. One possible solution would be designing an FMF-based circulator, which would avoid the core mismatch loss between the SMF and FMF.

Liu and co-workers designed and fabricated a graded-index FMF (GI-FMF) for high temperature and spatial resolution Raman DTS [50]. Under the overfilled launch condition, corresponding to the case when the spot size of the beam is larger than the fiber core radius, the GI-FMF-based Raman DTS achieves a temperature resolution of 1 °C at a distance of 25 km and a spatial resolution of 1.13 m. In contrast, an MMF-based Raman DTS achieves, at the same distance, a spatial resolution of 2.58 m and a temperature resolution of 0.7 °C [Fig. 12(a)]. The same GI-FMF-based Raman DTS achieves a temperature resolution of 4.7 °C at 25 km, under the QSM launch condition, compared to 6.9 °C at the same distance and the same spatial resolution of 1 m, using a standard SMF [Fig. 12(b)]. The results of this work are a clear example of using FMF as a compromise between SMF and MMF to offer DTS with a high spatial resolution as well as a desirable temperature resolution over a long measuring distance. Fiber optic distributed acoustic sensor (DAS), designed using the phase-sensitive optical time-domain reflectometry (ϕ-OTDR), is another important application that benefited from FMF. The functionality of DAS depends on the coherent interference of the Rayleigh signals reflected by scattering

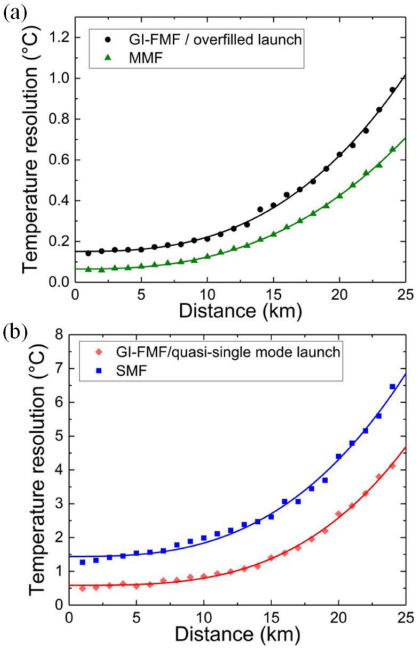

FIGURE 12. The temperature resolution profile using the GI-FMF and MMF (a) and GI-FMF and SMF (b) [50].

centers along the fiber [51]. As a result, SMF is the preferred platform for DAS because SMF supports propagating only the fundamental mode, which inhibits the interference noise originated from the higher-order modes. However, FMF operating in a QSM state can improve the SNR of DAS by allowing pumping higher optical powers, and meanwhile, it relatively acts as SMF by exciting only the fundamental mode into the FMF.

Mao *et al.* showed that the higher SNR offered by an FMF enables higher resolution and sensing range compared to a SMF, for DAS application [21]. In their investigations, the authors used a two-mode fiber (TMF) working in a QSM state. They reported that the TMF-based DAS recognizes a vibration event, produced by a piezoelectric transducer (PZT) cylinder, using two input high power levels of 1.34 W and 1.94 W. In contrast, for the same input power levels, the SMF-based DAS fails to locate the position of the vibration source. Figures 13(a) and 13(b) show the differential Rayleigh signals [52] when using the QSM-operated-TMF and SMF at 1.94 W input power, respectively. Chen *et al.* also demonstrated an SNR improvement for a ϕ-OTDR DAS system by combining the backscattered Rayleigh signals of the different spatial modes in a TMF [53]. However, the work in [21], [53] should be extended to investigate the performance of DAS systems designed using FMFs that support propagating more than two modes. Such a generalized study may significantly increase the sensing range of the commercially available SMF-based DAS. As the FMF-based multi-parameter sensing concept described in Section III-A, the compromise FMF can also offer simultaneous measurands monitoring. This is typically achieved via utilizing an FMF in a QSM state to fulfill the requirements of SMF-based sensors, such as DAS. Mean-

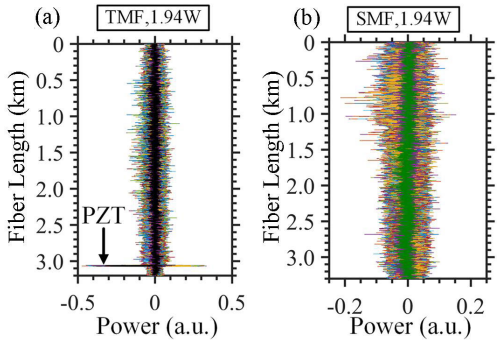

FIGURE 13. Differential Rayleigh signals when using the QSM-operated-TMF (a) and SMF (b), at 1.94 W input power [21].

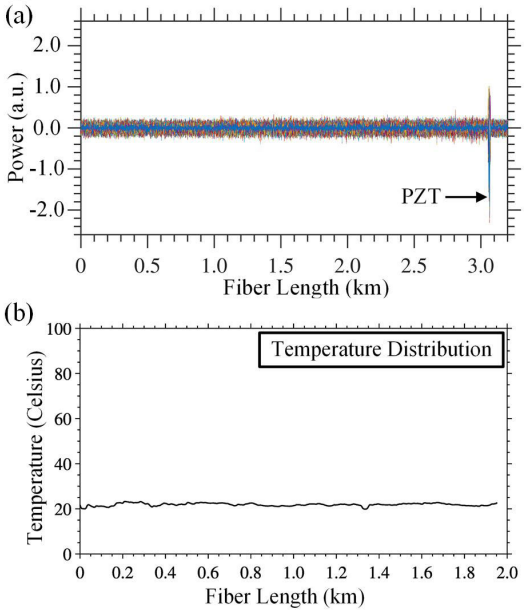

FIGURE 14. Differential Rayleigh signals (a) and temperature profile (b) measured using a QSM-operated-TMF in a hybrid DAS-DTS system [54].

while, high power can be injected into the FMF to realize the conditions of MMF-based sensors, such as DTS. For example, Ashry *et al.* utilized a TMF as a compromise between the standard SMF and MMF to design a hybrid DAS-DTS system [54]. Using the center-launching technique, the authors excited only the LP_{01} mode into the FMF to satisfy the operation requirements of the DAS and DTS. This design enables simultaneous measurements of vibrations produced by a PZT cylinder [Fig. 14(a)] and a temperature distribution of about 22 °C [Fig. 14(b)]. Although this work demonstrated an interesting and novel multi-parameter sensing approach using a TMF, it lacks characterizing the developed sensor thoroughly. For example, the temperature resolution along the fiber should be provided. Wu *et al.* reported utilizing a QSM-operated FMF to design a novel Raman-Brillouin system for simultaneous distributed curvature and temperature sensing [55]. By adding a Raman filter to a conventional BOTDA setup, the authors separated the Raman and Brillouin signals, in the wavelength-domain. The recorded Raman

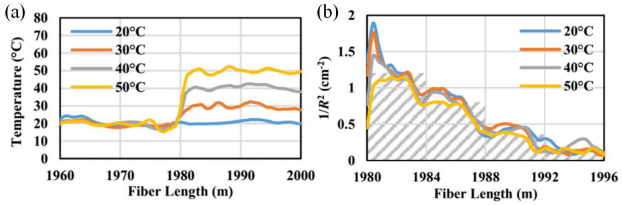

FIGURE 15. Measured temperature (a) and curvature (b) profiles of the last 40 m of the FMF [55].

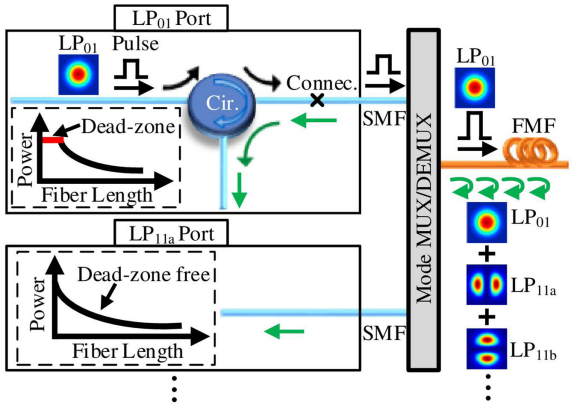

FIGURE 16. Dead-zone free OTDR using an FMF [56].

signal is initially used to measure the temperature profile along the FMF [Fig. 15(a)]. Meanwhile, with the help of the measured temperature reference, the Brillouin signal calculates the curvature distribution along the FMF [Fig. 15(b)]. A curvature/temperature measurement of a 0.33 cm^{-2}/1.3 °C accuracy with a spatial resolution of 1.5 m is attained, even at the end of the FMF. This design is very beneficial for a short sensing range ($\leq$2 km); however, the measurement accuracy values would degrade at longer sensing ranges ($\sim$10 km). Another interesting application of using FMF instead of standard SMF/MMF is the ability to sense within the OTDR dead-zone, as demonstrated in [56]. The OTDR dead-zone is defined as a distance along the fiber where the OTDR cannot detect defects or measure any event because of the high-power Fresnel reflections. By using a 2-mode FMF and a photonic lantern between the transmitter and the fiber, authors of [56] showed that it is possible to overcome the dead-zone caused by the Fresnel reflections at the fiber front facet. A general description of this design is described in Fig. 16, where an N-to-1 input-output mode MUX/DEMUX is added between the OTDR and the FMF. Light is launched in the LP_{01} mode port. The Fresnel reflection from the circulator and the FMF's front facet occur only for the injected LP_{01} mode, while the other recorded signals from the high-order mode ports are dead-zone free.

V. LIMITATIONS AND FUTURE PROSPECTS OF FMF-BASED OPTICAL SENSORS

Although FMF has proved the ability to design unique optical sensors, there are still some limitations when deploying FMF for multi-parameter sensing and large scale MDM sensing

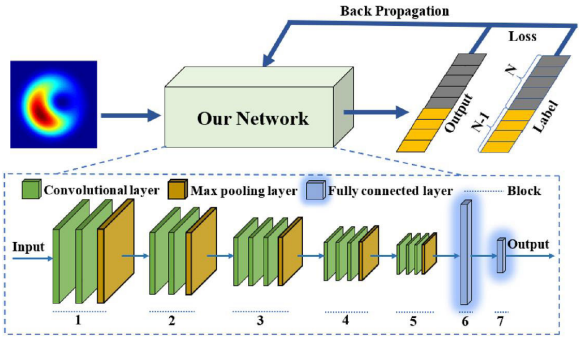

FIGURE 17. Schematic of the CNN used for the mode decomposition [58].

networks. FMF's intermodal coupling is considered the main drawback of using FMF in optical sensing [22]. In particular, intermodal coupling creates significant intensity and phase noise for the complex coefficients of the FMF modes, which degrade the performance of FMF-based sensors. The impact of intermodal coupling becomes severe as the number of spatial modes increases within an FMF. Consequently, in the literature, the multi-parameter sensing trials using an FMF are typically limited to monitoring two measurands. Additionally, the impact of intermodal coupling is accumulated as the modes travel along an FMF, which consequently limits the scale of MDM sensing networks.

Several conventional techniques have been reported to mitigate intermodal coupling in FMF, including MIMO processing [27] and adaptive optics [57]. However, such methods require using complex experimental setups and huge computational resources, especially for a large number of spatial modes. Recently, machine learning (ML) methods have been introduced to perform mode decomposition in FMF. Such ML-based techniques would, in real-time, facilitate calculating FMF's mode transfer matrix, which can then be inverted to overcome the effect of intermodal coupling completely [26]. For example, An *et al.* reported a deep-learning-based technique to determine the modal amplitudes and phases in 3-mode and 5-mode optical fibers [58]. A convolutional neural network (CNN) is trained with simulated intensity profiles of the modes supported by the FMF, while the network performance is evaluated using simulated and real beam profiles. The used CNN comprises 7 blocks where the filter size of the first convolutional is set to $3 \times 3 \times 1$, as the input intensity images are grayscaled [Fig. 17]. The authors reported average prediction errors for the modal amplitude weights of 0.5% and 1% for the 3-mode and 5-mode FMFs, respectively, when using the simulated data. The reported average prediction errors for the modal phases are 0.7% (1.3%) for the 3-mode (5-mode) FMF, using the simulated data. The average amplitude weights and phase errors increase to 2.3% and 4.9%, respectively, for a 10-mode FMF. In the future, we believe that ML methods will play a crucial role in developing FMF-based sensors. Given the high accuracy of mode decomposition realized by ML, more than two measurands can be simultaneously

sensed using FMF. Notably, in real-time, the intensity/phase of the individual modes would be well monitored and linked to the sensing parameters. Additionally, the ML-based mode decomposition algorithms would help compensate for the impact of intermodal coupling within an MDM sensing network, expanding the scale of such networks. Alternatively, without mode decomposition, ML would directly link the changes of the modes' intensities, patterns, spectra, phases, etc. with different measurands, which might open up new research directions.

VI. CONCLUSION

The progressive development of FMF-based sensors has mainly resulted from the FMF's unique capabilities, which cannot be offered by standard SMF/MMF. In this review, we have provided a comprehensive summary of the different types and operation principles of FMF sensors. We have initially highlighted that various modes propagating within an FMF have different n_{eff} values and spatial distributions. Such FMF characteristics cause different modes to interact differently with sensing measurands. Consequently, FMF resolves long-standing challenges, such as simultaneous distributed sensing of temperature and strain. By scanning sensing interrogation signals in mode-space, FMF can also reconstruct spatial distributions of chemicals that diffuse into the FMF. We have further presented the trials of using FMF as a compromise between standard SMF and MMF to design FMF-based sensors with higher SNR and spatial resolution. For example, a QSM-operated FMF can be used to design DAS and DTS with improved specifications, compared to the counterparts designed using standard SMF and MMF, respectively. Finally, we have discussed intermodal coupling as the main limitation of FMF-based sensors; however, ML methods are expected to efficiently resolve this challenge in the near future.

ACKNOWLEDGMENT

(Islam Ashry, Yuan Mao, Abderrahmen Trichili, and Biwei Wang contributed equally to this work.)

REFERENCES

[1] B. Culshaw and A. Kersey, "Fiber-optic sensing: A historical perspective," *J. Lightw. Technol.*, vol. 26, no. 9, pp. 1064–1078, May 1, 2008.

[2] X. Bao and L. Chen, "Recent progress in distributed fiber optic sensors," *Sensors*, vol. 12, no. 7, pp. 8601–8639, Jun. 2012.

[3] T. Yamate, G. Fujisawa, and T. Ikegami, "Optical sensors for the exploration of oil and gas," *J. Lightw. Technol.*, vol. 35, no. 16, pp. 3538–3545, Aug. 15, 2017.

[4] A. Barrias, J. Casas, and S. Villalba, "A review of distributed optical fiber sensors for civil engineering applications," *Sensors*, vol. 16, no. 5, p. 748, May 2016.

[5] A. Grillet, D. Kinet, J. Witt, M. Schukar, K. Krebber, F. Pirotte, and A. Depre, "Optical fiber sensors embedded into medical textiles for healthcare monitoring," *IEEE Sensors J.*, vol. 8, no. 7, pp. 1215–1222, Jul. 2008.

[6] A. Kersey and A. Dandridge, "Applications of fiber-optic sensors," *IEEE Trans. Compon., Hybrids, Manuf. Technol.*, vol. 13, no. 1, pp. 137–143, Mar. 1990.

[7] I. Ashry, Y. Mao, Y. Al-Fehaid, A. Al-Shawaf, M. Al-Bagshi, S. Al-Brahim, T. K. Ng, and B. S. Ooi, "Early detection of red palm weevil using distributed optical sensor," *Sci. Rep.*, vol. 10, no. 1, pp. 1–8, Dec. 2020.

[8] N. Sabri, S. Aljunid, M. Salim, and S. Fouad, "Fiber optic sensors: Short review and applications," in *Recent Trends in Physics of Material Science and Technology*. Singapore: Springer, 2015, pp. 299–311.

[9] J. Villatoro, V. Finazzi, V. P. Minkovich, V. Pruneri, and G. Badenes, "Temperature-insensitive photonic crystal fiber interferometer for absolute strain sensing," *Appl. Phys. Lett.*, vol. 91, no. 9, Aug. 2007, Art. no. 091109.

[10] Y. Liu, B. Liu, X. Feng, W. Zhang, G. Zhou, S. Yuan, G. Kai, and X. Dong, "High-birefringence fiber loop mirrors and their applications as sensors," *Appl. Opt.*, vol. 44, no. 12, pp. 2382–2390, Apr. 2005.

[11] L. Palmieri, "Coupling mechanism in multimode fibers," *Proc. SPIE*, vol. 9009, Feb. 2014, Art. no. 90090G.

[12] T. Qiu, I. Ashry, A. Wang, and Y. Xu, "Adaptive mode control in 4- and 17-mode fibers," *IEEE Photon. Technol. Lett.*, vol. 30, no. 11, pp. 1036–1039, Jun. 1, 2018.

[13] A. Li, Y. Wang, Q. Hu, and W. Shieh, "Few-mode fiber based optical sensors," *Opt. Express*, vol. 23, no. 2, pp. 1139–1150, Jan. 2015.

[14] I. Ashry, A. Wang, and Y. Xu, "Mode-division-multiplexing of absorption-based fiber optical sensors," *Opt. Express*, vol. 24, no. 5, pp. 5186–5202, 2016.

[15] C. Wang, Z. Huang, G. Li, S. Zhang, J. Zhao, N. Zhao, H. Cai, and Y. Zhang, "Simultaneous temperature and strain measurements using polarization-maintaining few-mode Bragg gratings," *Sensors*, vol. 19, no. 23, p. 5221, Nov. 2019.

[16] X. Zhan, Y. Liu, M. Tang, L. Ma, R. Wang, L. Duan, L. Gan, C. Yang, W. Tong, and S. Fu, "Few-mode multicore fiber enabled integrated Mach-Zehnder interferometers for temperature and strain discrimination," *Opt. Express*, vol. 26, no. 12, pp. 15332–15342, 2018.

[17] K.-I. Kitayama and N.-P. Diamantopoulos, "Few-mode optical fibers: Original motivation and recent progress," *IEEE Commun. Mag.*, vol. 55, no. 8, pp. 163–169, Aug. 2017.

[18] P. Sillard, M. Bigot-Astruc, and D. Molin, "Few-mode fibers for Mode-Division-Multiplexed systems," *J. Lightw. Technol.*, vol. 32, no. 16, pp. 2824–2829, Aug. 15, 2014.

[19] I. Ashry, A. Wang, and Y. Xu, "Mode-based reconstruction of chemical distributions in optical fibers," *IEEE J. Sel. Topics Quantum Electron.*, vol. 23, no. 2, pp. 229–237, Mar. 2017.

[20] M. Wang, H. Wu, M. Tang, Z. Zhao, Y. Dang, C. Zhao, R. Liao, W. Chen, S. Fu, C. Yang, W. Tong, P. P. Shum, and D. Liu, "Few-mode fiber based Raman distributed temperature sensing," *Opt. Express*, vol. 25, no. 5, pp. 4907–4916, 2017.

[21] Y. Mao, I. Ashry, M. S. Alias, T. K. Ng, F. Hveding, M. Arsalan, and B. S. Ooi, "Investigating the performance of a few-mode fiber for distributed acoustic sensing," *IEEE Photon. J.*, vol. 11, no. 5, pp. 1–10, Oct. 2019.

[22] S. Ö. Arik, D. Askarov, and J. M. Kahn, "Effect of mode coupling on signal processing complexity in mode-division multiplexing," *J. Lightw. Technol.*, vol. 31, no. 3, pp. 423–431, Feb. 1, 2013.

[23] M. B. Shemirani, W. Mao, R. A. Panicker, and J. M. Kahn, "Principal modes in graded-index multimode fiber in presence of spatial- and polarization-mode coupling," *J. Lightw. Technol.*, vol. 27, no. 10, pp. 1248–1261, May 15, 2009.

[24] A. A. Juarez, E. Krune, S. Warm, C. A. Bunge, and K. Petermann, "Modeling of mode coupling in multimode fibers with respect to bandwidth and loss," *J. Lightw. Technol.*, vol. 32, no. 8, pp. 1549–1558, Apr. 15, 2014.

[25] S. Rommel, J. Manuel D. Mendinueta, W. Klaus, J. Sakaguchi, J. J. V. Olmos, Y. Awaji, I. T. Monroy, and N. Wada, "Few-mode fiber, splice and SDM component characterization by spatially-diverse optical vector network analysis," *Opt. Express*, vol. 25, no. 19, pp. 22347–22361, Sep. 2017.

[26] J. Carpenter, B. J. Eggleton, and J. Schröder, "110×110 optical mode transfer matrix inversion," *Opt. Express*, vol. 22, no. 1, pp. 96–101, 2014.

[27] R. Ryf, S. Randel, A. H. Gnauck, C. Bolle, A. Sierra, S. Mumtaz, and M. Esmaeelpour, "Mode-division multiplexing over 96 km of few-mode fiber using coherent 6×6 MIMO processing," *J. Lightw. Technol.*, vol. 30, no. 4, pp. 521–531, Feb. 15, 2012.

[28] K.-P. Ho and J. M. Kahn, *Optical Fiber Telecommunications VIB: Mode Coupling and its Impact on Spatially Multiplexed Systems*. Amsterdam, The Netherlands: Elsevier, 2013, ch. 11.

[29] W. Jin, W. C. Michie, G. Thursby, M. Konstantaki, and B. Culshaw, "Simultaneous measurement of strain and temperature: Error analysis," *Opt. Eng.*, vol. 36, pp. 598–609, Feb. 1997.

[30] H. Z. Yang, M. M. Ali, M. R. Islam, K.-S. Lim, D. S. Gunawardena, and H. Ahmad, "Cladless few mode fiber grating sensor for simultaneous refractive index and temperature measurement," *Sens. Actuators A, Phys.*, vol. 228, pp. 62–68, Jun. 2015.
[31] J.-M. Savolainen, L. Grüner-Nielsen, P. Kristensen, and P. Balling, "Measurement of effective refractive-index differences in a few-mode fiber by axial fiber stretching," *Opt. Express*, vol. 20, no. 17, pp. 18646–18651, 2012.
[32] Y. Weng, E. Ip, Z. Pan, and T. Wang, "Single-end simultaneous temperature and strain sensing techniques based on Brillouin optical time domain reflectometry in few-mode fibers," *Opt. Express*, vol. 23, no. 7, pp. 9024–9039, 2015.
[33] A. Li, Q. Hu, X. Chen, B. Y. Kim, and W. Shieh, "Characterization of distributed modal birefringence in a few-mode fiber based on Brillouin dynamic grating," *Opt. Lett.*, vol. 39, no. 11, pp. 3153–3156, Jun. 2014.
[34] E. Chehura, S. W. James, and R. P. Tatam, "Temperature and strain discrimination using a single tilted fibre Bragg grating," *Opt. Commun.*, vol. 275, no. 2, pp. 344–347, Jul. 2007.
[35] D.-P. Zhou, L. Wei, W.-K. Liu, Y. Liu, and J. W. Y. Lit, "Simultaneous measurement for strain and temperature using fiber Bragg gratings and multimode fibers," *Appl. Opt.*, vol. 47, no. 10, pp. 1668–1672, Apr. 2008.
[36] Y. Zhao, C. Wang, G. Yin, B. Jiang, K. Zhou, C. Mou, Y. Liu, L. Zhang, and T. Wang, "Simultaneous directional curvature and temperature sensor based on a tilted few-mode fiber Bragg grating," *Appl. Opt.*, vol. 57, no. 7, pp. 1671–1678, Mar. 2018.
[37] V. Bhatia, "Applications of long-period gratings to single and multi-parameter sensing," *Opt. Express*, vol. 4, no. 11, pp. 457–466, May 1999.
[38] M. Song, S. B. Lee, S. S. Choi, and B. Lee, "Simultaneous measurement of temperature and strain using two fiber Bragg gratings embedded in a glass tube," *Opt. Fiber Technol.*, vol. 3, no. 2, pp. 194–196, Apr. 1997.
[39] M. A. Soto, T. Nannipieri, A. Signorini, A. Lazzeri, F. Baronti, R. Roncella, G. Bolognini, and F. Di Pasquale, "Raman-based distributed temperature sensor with 1 m spatial resolution over 26km SMF using low-repetition-rate cyclic pulse coding," *Opt. Lett.*, vol. 36, no. 13, pp. 2557–2559, 2011.
[40] Y. Mao, I. Ashry, F. Hveding, A. Y. Bukhamsin, Y. Hong, T. K. Ng, and B. S. Ooi, "Simultaneous distributed acoustic and temperature sensing using a multimode fiber," *IEEE J. Sel. Topics Quantum Electron.*, vol. 26, no. 4, pp. 1–7, Jul. 2020.
[41] Y. Muanenda, C. J. Oton, S. Faralli, T. Nannipieri, A. Signorini, and F. Di Pasquale, "Hybrid distributed acoustic and temperature sensor using a commercial off-the-shelf DFB laser and direct detection," *Opt. Lett.*, vol. 41, no. 3, pp. 587–590, Feb. 2016.
[42] A. Minardo, E. Catalano, A. Coscetta, and L. Zeni, "Dual wavelength Botda for strain/temperature discrimination," in *Sensors Microsystems*, A. Leone, A. Forleo, L. Francioso, S. Capone, P. Siciliano, and C. Di Natale, Eds. Cham, Switzerland: Springer, 2018, pp. 25–28.
[43] S. Korposh, S. James, S.-W. Lee, and R. Tatam, "Tapered optical fibre sensors: Current trends and future perspectives," *Sensors*, vol. 19, no. 10, p. 2294, May 2019.
[44] A. Marzuki, A. C. Pratiwi, and V. Suryanti, "Evanescent wave absorption based fiber sensor for measuring glucose solution concentration," in *Proc. IOP Conf., Mater. Sci. Eng.*, vol. 333, no. 1. Bristol, U.K.: IOP Publishing, 2018, Art. no. 012016.
[45] P. L. Swart and A. A. Chtcherbakov, "Study of hydrogen diffusion in boron/germanium codoped optical fiber," *J. Lightw. Technol.*, vol. 20, no. 11, pp. 1933–1941, Nov. 2002.
[46] P. J. Lemaire, "Reliability of optical fibers exposed to hydrogen: Prediction of long-term loss increases," *Opt. Eng.*, vol. 30, no. 6, pp. 780–790, 1991.
[47] R. Atkins, V. Miuahi, and W. Reed, "High pressure H: Loading as a rechnique for achieving ultrahigh UV photosensitivity and themlal sensitivity in GeOz dQped oplical fibers," *Electron. Lett.*, vol. 29, no. 13, p. 1191, 1993.
[48] B. Malo, D. C. Johnson, F. Bilodeau, J. Albert, and K. O. Hill, "Effective index drift from molecular hydrogen diffusion in hydrogen-loaded optical fibres and its effect on Bragg grating fabrication," *Electron. Lett.*, vol. 30, no. 5, pp. 442–444, Mar. 1994.
[49] G. Agrawal, *Nonlinear Fiber Optics*. New York, NY, USA: Academic, 2003.
[50] Y. Liu, L. Ma, C. Yang, W. Tong, and Z. He, "Long-range Raman distributed temperature sensor with high spatial and temperature resolution using graded-index few-mode fiber," *Opt. Express*, vol. 26, no. 16, pp. 20562–20571, 2018.
[51] X. Bao, D.-P. Zhou, C. Baker, and L. Chen, "Recent development in the distributed fiber optic acoustic and ultrasonic detection," *J. Lightw. Technol.*, vol. 35, no. 16, pp. 3256–3267, Aug. 15, 2017.
[52] I. Ashry, Y. Mao, M. S. Alias, T. K. Ng, F. Hveding, M. Arsalan, and B. S. Ooi, "Normalized differential method for improving the signal-to-noise ratio of a distributed acoustic sensor," *Appl. Opt.*, vol. 58, no. 18, pp. 4933–4938, 2019.
[53] M. Chen, A. Masoudi, F. Parmigiani, and G. Brambilla, "Distributed acoustic sensor based on a two-mode fiber," *Opt. Express*, vol. 26, no. 19, pp. 25399–25407, 2018.
[54] I. Ashry, Y. Mao, T. K. Ng, F. Hveding, M. Arsalan, and B. S. Ooi, "Hybrid distributed acoustic-temperature sensing using a few-mode fiber," *Proc. SPIE*, vol. 11287, Mar. 2020, Art. no. 112870N.
[55] H. Wu, M. Tang, M. Wang, C. Zhao, Z. Zhao, R. Wang, R. Liao, S. Fu, C. Yang, and W. Tong, "Few-mode optical fiber based simultaneously distributed curvature and temperature sensing," *Opt. Express*, vol. 25, no. 11, pp. 12722–12732, 2017.
[56] Y. Mao, I. Ashry, B. Wang, F. Hveding, A. Y. Bukhamseen, K. T. Ng, and B. S. Ooi, "Sensing within the OTDR dead-zone using a two-mode fiber," *Opt. Lett.*, vol. 45, no. 11, pp. 2969–2972, 2020.
[57] A. Li, Y. Wang, Q. Hu, D. Che, X. Chen, and W. Shieh, "Measurement of distributed mode coupling in a few-mode fiber using a reconfigurable Brillouin OTDR," *Opt. Lett.*, vol. 39, no. 22, pp. 6418–6421, 2014.
[58] Y. An, L. Huang, J. Li, J. Leng, L. Yang, and P. Zhou, "Learning to decompose the modes in few-mode fibers with deep convolutional neural network," *Opt. Express*, vol. 27, no. 7, pp. 10127–10137, 2019.

ISLAM ASHRY (Senior Member, IEEE) received the B.S. and M.S. degrees from Alexandria University, Alexandria, Egypt, in 2003 and 2007, respectively, and the Ph.D. degree from the Virginia Polytechnic Institute and State University (Virginia Tech), Blacksburg, VA, USA, in 2012. He is currently a Research Scientist with the Photonics Laboratory, KAUST. His research interests include optical sensing, mode-division-multiplexing, fluorescence dynamics, nano-patterning, plasmon sensing, fiber optics, and optical networks. He is a member of SPIE.

YUAN MAO (Senior Member, IEEE) received the B.S. degree in fundamental science from Tsinghua University, Beijing, China, in 2007, and the Ph.D. degree in electronic and information engineering from The Hong Kong Polytechnic University, Hong Kong, China, in 2013. He is currently a Research Scientist with the Photonics Laboratory, KAUST. His research interests include distributed fiber sensors, fiber optical communications, and wireless optical communications. He is a member of OSA, SPIE, and IoP.

ABDERRAHMEN TRICHILI (Member, IEEE) received the Diplôme d'Ingénieur and Ph.D. degrees in information and communication technology from the L'École Supérieure des Communications de Tunis (SUP'COM), Tunisia, in 2013 and 2017, respectively. He is currently a Postdoctoral Fellow with the CEMSE Division, King Abdullah University of Science and Technology (KAUST). His current research interests include space-division multiplexing, orbital angular momentum multiplexing, and optical wireless communication systems.

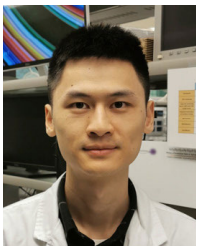

BIWEI WANG received the B.S. degree in optoelectronic information engineering from the Huazhong University of Science and Technology, Wuhan, China, in 2015. He is currently pursuing the Ph.D. degree in electronic and information engineering with The Hong Kong Polytechnic University. He worked as a Research Assistant at the Department of Electronic and Information Engineering, The Hong Kong Polytechnic University, from 2015 to 2016. His research interests include distributed optical fiber sensors and applications of machine learning techniques in optical fiber sensors.

TIEN KHEE NG (Senior Member, IEEE) received the M.Eng. and Ph.D. degrees from Nanyang Technological University (NTU), Singapore, in 2001 and 2005, respectively. He was a Test Engineer with Hewlett-Packard Singapore, from 1997 to 1998, a Member of the Technical Staff with Tinggi Technologies, from 2004 to 2006, and a Research Fellow with NTU, until 2009. He is currently a Principal Research Scientist with the Ooi Group, King Abdullah University of Science and Technology (KAUST), Thuwal, Saudi Arabia. As a Co-Principal Investigator, he was responsible for innovation in MBE-grown nanostructures devices and in laser devices with the KACST Technology Innovation Center on Solid-State Lighting, KAUST, where he realized wide-bandgap nitride quantum confined and nanowires structures for light-emitters technology, optical wireless communications, and energy harvesting. He is a member of SPIE and IoP and a Senior Member of The Optical Society (OSA).

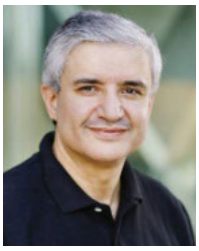

MOHAMED-SLIM ALOUINI (Fellow, IEEE) received the Ph.D. degree in electrical engineering from the California Institute of Technology (Caltech), Pasadena, CA, USA, in 1998. He served as a Faculty Member with the University of Minnesota, Minneapolis, MN, USA, and Texas A&M University at Qatar, Doha, Qatar, before joining the King Abdullah University of Science and Technology (KAUST), Thuwal, Saudi Arabia, as a Professor of Electrical Engineering, in 2009. His current research interests include modeling, design, and performance analysis of wireless communication systems.

BOON S. OOI (Senior Member, IEEE) received the Ph.D. degree from the University of Glasgow, U.K., in 1994. He is currently a Professor of Electrical Engineering with the King Abdullah University of Science and Technology (KAUST). He joined KAUST from Lehigh University, USA, in 2009. His recent research is concerned with the study of III-nitride-based materials and devices and lasers for applications, such as solid-state lighting, optical sensing, visible light and underwater wireless optical communications, and energy harvesting devices. He is a Fellow of the U.S. National Academy of Inventors (NAI), OSA, SPIE, and IoP, U.K. He has served on the Technical Program Committee of CLEO, IPC, ISLC, and IEDM. He serves on the Editorial Board of *Optics Express* and the IEEE PHOTONICS JOURNAL.